PAPER

Check for updates

Electrocatalytic properties of a carbothermically obtained composite based on vanadium nitridophosphide in the hydrogen evolution, oxygen evolution, and oxygen reduction reactions

Denys O. Mazur, [ID] Olena O. Pariiska, Yaroslav I. Kurys [ID] *
and Vyacheslav G. Koshechko

Hydrogen evolution reaction (HER), oxygen evolution reaction (OER), and oxygen reduction reaction (ORR) are the key electrochemical processes of hydrogen energy. Transition metal phosphides, nitrides, carbides, chalcogenides and their composites are promising non-precious metal electrocatalysts for these processes. Catalysts based on so-called early d-metal compounds, particularly V, attract less attention compared to those based on late transition metals (Ni, Co, Fe, *etc.*), which can generally be explained by their less competitive catalytic characteristics. However, combining V-containing compounds with late transition metal compounds or doping vanadium compounds with late d-metals allows for a significant increase in the performance of V-containing systems. This possibility, as well as the inherent electroconductive properties, ability to function in a wide pH range, and corrosion resistance of a number of vanadium compounds, determine the prospect of their use to create stable and effective electrocatalysts for HER, OER, and ORR. This work firstly shows that pyrolysis of polyaniline doped with phosphoric acid together with sodium metavanadate allows the production composite electrocatalyst for HER, OER and ORR based on vanadium nitridophosphide and N, P-co-doped carbon (V_5NP_3/N, P-C). The proposed approach is straightforward to implement and avoids the need for ammonia and toxic phosphorus compounds. It was found that in terms of its activity in all the studied processes, V_5NP_3/N, P-C exceeds the vast majority of known catalysts based on vanadium nitride or phosphide (provided that there are no additional late d-metals in their composition), and is characterized in HER by a Tafel slope (b) of $\sim$91 mV dec^{-1} and an overpotential at 10 mA cm^{-2} (η_{10}) of $\sim$304 and 325 mV (in 1.0 M NaOH and 0.5 M H_2SO_4, respectively), in OER – η_{10} of $\sim$290 mV and b of $\sim$241 mV dec^{-1}, in ORR – E_{onset} of $\sim$890 mV, $E_{1/2}$ of $\sim$820 mV and b of $\sim$61 mV dec^{-1}. Considering the high functional characteristics of V_5NP_3/N, P-C in HER, OER and ORR, as a composite based on an early d-metal compound, it can be used, in our opinion, for the formation within the framework of the proposed approach of competitive hybrid electrocatalysts with late d-metals or their compounds.

Introduction

The Hydrogen Evolution Reaction (HER), Oxygen Evolution Reaction (OER), and Oxygen Reduction Reaction (ORR) play a key role in clean and renewable energy technologies.[1–3] Specifically, HER and OER provide the basis for electrolytic water splitting – a technology considered the most promising for obtaining high-purity molecular hydrogen due to its environmental friendliness and virtually unlimited water resources. Meanwhile, ORR is implemented in fuel cells and metal–air batteries – devices that provide efficient energy conversion with low environmental pollution. A necessary prerequisite for the

practical implementation of HER, OER, and ORR is the use of electrocatalysts to reduce the energy barrier of these reactions.[3] Catalysts based on Pt[2,4] (HER, ORR) and IrO_2 or RuO_2 (ref. 5 and 6) (OER) allows for a significant reduction in the overpotential of the respective electrochemical processes, which is caused by electrode polarization. However, despite the efficiency of such catalysts, the high cost of noble metals, their limited resources, and, often, the insufficient stability of the catalysts cause extensive research to find new, much cheaper systems that, in the absence of noble metals, can exhibit high activity in HER, OER, and ORR and stability during long-term operation.

Transition metals (Ni, Co, Fe, Mo, *etc.*) are much cheaper compared to noble metals and have significant proven reserves. This fact, as well as the high electrocatalytic characteristics in HER, OER, and ORR of a number of d-metal compounds

L.V. Pisarzhevskii Institute of Physical Chemistry of the National Academy of Sciences of Ukraine, 31 Nauky Pr., Kyiv 03028, Ukraine. E-mail: yarkurys@ukr.net

(carbides, nitrides, phosphides, chalcogenides, hydroxides, *etc.*) established in numerous studies, allows them to be considered as an attractive alternative to noble metal-based catalysts.[2,7–16] In this context, the vast majority of research is focused on compounds of so-called late transition metals (particularly Ni, Co, Fe) or their composites. At the same time, catalysts based on early d-metal compounds, particularly V, receive less attention, which can generally be explained by their less competitive catalytic characteristics in HER, OER, and ORR.[17] However, combining V-containing compounds with late transition metal compounds (co-catalysts), using the strategy of doping vanadium compounds with late d-metals and non-metal atoms, creating composites with N-doped carbon nanomaterials, *etc.*, allows for a significant increase in the performance of V-containing systems in these processes. This, along with the inherent electroconductive properties, ability to function in a wide pH range, and corrosion resistance (particularly of VN, V carbides, and V phosphides), determines the prospect of their use as stable and effective electrocatalysts for HER, OER, and ORR.[17] Considering this, the development of new electrocatalysts based on vanadium compounds is a relevant task.

Recently, we have shown that high-temperature treatment in an inert atmosphere of polyaniline doped with phosphoric acid ($PAni \cdot H_3PO_4$) together with a d-metal salt (Co, Ni, Mo, or Fe) allows for the production of composites based on particles of the corresponding d-metal phosphides and carbon co-doped with nitrogen and phosphorus (Met_xP_y/N, P-C, where Met = Co, Ni, Mo, or Fe) as electrocatalysts for HER, OER, and ORR.[18,19] Considering the attractiveness of the proposed approach (simplicity of implementation, low cost of starting reagents, absence of the need to use highly toxic phosphorus compounds), it was of interest to ascertain the possibility of its implementation for obtaining an analogous composite based on vanadium phosphide(s) particles (an early d-metal) and to evaluate the electrocatalytic properties of such a composite in HER, OER, and ORR.

In this work, such a possibility was investigated, and it was shown that the pyrolysis of $PAni \cdot H_3PO_4$ (as a source of phosphorus, nitrogen, and carbon) together with sodium metavanadate unexpectedly leads not to the formation of a composite of carbon co-doped with nitrogen and phosphorus with V phosphide(s) particles, but with particles of vanadium nitridophosphide – V_5NP_3 (V_5NP_3/N, P-C). In the work, assumptions regarding the formation mechanism of such a composite are made, the main characteristics of V_5NP_3/N, P-C as an electrocatalyst for HER, OER, and ORR are determined, and a comparison of the electrocatalytic properties of the obtained composite with known catalysts based on vanadium phosphides and nitride is also carried out. To the best of our knowledge, V_5NP_3-containing composites, as well as the electrocatalytic properties of V_5NP_3 or hybrid materials based on it, have not been previously discussed in the literature.

Experimental section

Phosphoric acid-doped polyaniline ($PAni \cdot H_3PO_4$) was obtained *via* oxidative polymerization of aniline in an aqueous solution of 2 M H_3PO_4 (SI).[18,20]

Synthesis of the composite based on N, P-doped carbon and vanadium nitridophosphide particles. 1.00 g of $PAni \cdot H_3PO_4$ was dispersed in 20 mL of ethanol (10 min), and an aqueous solution of 0.28 g $NaVO_3 \cdot H_2O$ (10 wt% metal relative to the doped polymer) was added to the dispersion. The mixture was air-dried, and the dry residue was transferred to a ceramic crucible, which was placed in a tube furnace. The furnace was purged with argon for 15 min, after which the residue was heat-treated in an argon flow at 900 °C for 3 hours, followed by cooling the obtained carbonization product to room temperature in an argon atmosphere. The pyrolysis product was treated with 0.5 M H_2SO_4 (80 °C, 1 hour), then washed with water on a filter (to pH ~7) and dried in a drying oven at 90 °C.

N, P-doped carbon (N, P-C) obtained in an analogous manner but in the absence of $NaVO_3 \cdot H_2O$ (SI), as well as Pt/C catalyst (20% Pt on Vulcan XC-72R, FuelCell Store), were used for comparison in electrocatalytic studies.

XRD-patterns of the composite and its precursor were recorded on a D8 ADVANCE diffractometer (Bruker) using filtered CuKα radiation ($\lambda = 0.154$ nm). Samples were pressed onto a non-diffracting silicon substrate. Morphology of the composite was investigated by scanning electron microscopy (SEM) using a Tescan Mira 3 LMU microscope (accelerating voltage 10 kV), and its elemental composition was determined by energy-dispersive X-ray spectroscopy (EDX) data (Bruker XFlash detector). The studies of the obtained composites by transmission electron microscopy (TEM) were carried out on a TEM-125K microscope (Selmi), accelerating voltage 100 kV. The Raman spectra of the samples, deposited on a silicon substrate, were recorded on a Renishaw spectrometer ($\lambda = 514$ nm). XPS measurements were performed on a PHI 5600 spectrometer equipped with a monochromatic Al K$_\alpha$ source. The instrument work function was calibrated to give the binding energy (BE) of 84 eV for the Au $4f_{7/2}$ line for metallic gold and the spectrometer dispersion was adjusted to give a BE of 932.6 eV for the Cu $2p_{3/2}$ line of metallic copper. Survey spectra were acquired at a pass energy of 93.9 eV with a step size of 0.2 eV. Prior to analysis, the samples were not pre-etched with the ion gun. Data processing was carried out using CasaXPS 2.3.15 software with the Voigt function (Gaussian/Lorentzian ratio of 70 : 30). The number of fitted components was limited to the minimum required to describe the spectrum, and their full width at half maximum did not exceed the physically reasonable values for the respective elements. Peak positions were determined with an accuracy of ±0.2 eV. The C 1s photoemission line was used as a reference for energy calibration.

Polarization curves for HER and OER were recorded on a VersaSTAT4-200 potentiostat/galvanostat (Princeton Applied Research) using an undivided electrochemical cell: working electrode – glass carbon (GC) disc with a visible surface area of 0.03 cm^2; auxiliary electrode – platinum wire; reference electrode – Ag/AgCl in 3 M NaCl. Polarization curves were *iR*-corrected. The electrocatalyst loading was ~1.15 mg cm^{-2}. ORR studies were conducted in the same electrochemical cell on a rotating ring-disk electrode (RRDE 636 A, Princeton Applied Research) in conjunction with a bipotentiostat (MTech BP-10, MTechLab). The visible surface area of the GC disc was 0.2375 cm^2, and the Pt ring

was 0.1866 cm^2. The electrocatalyst loading was ∼0.29 mg cm^{-2}. Current density was determined considering the geometric surface area of the electrode. All potential values are reported relative to the reversible hydrogen electrode (RHE), $E_{RHE} = E_{Ag/AgCl} + 0.059\,pH + E°_{Ag/AgCl}$, $E°_{Ag/AgCl} = 198$ mV.

Preparation of GC electrodes before electrochemical studies involved polishing them with suspensions of diamond particles (1.0 μm) and Al$_2$O$_3$ nanoparticles (0.05 μm), followed by ultrasonic cleaning in a water–ethanol mixture (1 : 1 vol.) and distilled water. Modification of GC electrodes with electrocatalysts was carried out by applying 2 μL of a dispersion containing 2 mg of the obtained composite (or N, P-C or Pt/C), 48 μL of EtOH, and 8 μL of a 5% Nafion solution in a mixture of low molecular weight aliphatic alcohols, followed by air-drying of the modified electrodes.

Tafel slope (b) was calculated using eqn S1 (SI) from the linear regions of the corresponding Tafel curves. When analyzing data obtained by the RRDE method, eqn S2–S4 (SI) were used to calculate the number of electrons (n) participating in the reduction of 1 oxygen molecule, the hydrogen peroxide yield (H$_2$O$_2$%), and to determine the half-wave potential ($E_{1/2}$).

The electrochemical impedance spectroscopy (EIS) measurements were performed using a μAUTOLAB III/FRA2 instrument (ECO CHEMIE) in a three-electrode cell. EIS spectra were recorded in the 500 kHz–0.05 Hz frequency range with an amplitude of 10 mV.

Results and discussions

As noted above, the pyrolysis of PAni·H$_3$PO$_4$ with Ni, Co, Mo, or Fe salts yields composites containing phosphide particles of the corresponding d-metals.[18,19] However, as shown in the XRD-pattern in Fig. 1a, under identical heat treatment conditions for the precursor based on PAni·H$_3$PO$_4$ and NaVO$_3$·H$_2$O, a composite with a different metal-containing crystalline phase is formed: vanadium nitridophosphide (V$_5$NP$_3$) [PDF 021-0616].[21] The obtained composite is hereinafter referred to as V$_5$NP$_3$/N, P-C, considering the obvious presence of carbon in its composition (due to polyaniline carbonization) and the doping of the carbon matrix with nitrogen and phosphorus atoms,

which typically occurs during the pyrolysis of N, P-containing polymers in the precursor composition.[18,22–24]

Due to the amorphous state of carbon, its presence in the composite is practically undetectable by a characteristic peak in the XRD-pattern at 26.5°. However, it is unequivocally confirmed by the results of Raman spectroscopy on V$_5$NP$_3$/N, P-C. In the Raman spectrum of V$_5$NP$_3$/N, P-C (Fig. 1b, curve 2), similar to N, P-C (Fig. 1b, curve 1), two intense peaks are present with maxima at approximately 1349 and 1596 cm^{-1}. These are characteristics of carbonaceous materials and correspond, respectively, to the disorder-induced phonon mode (D-band), which is caused by defects in the carbon framework, and the graphitic G-band. The relatively high intensity ratio of $I_{(D)}/I_{(G)}$, which is 0.88, indicates a significant degree of disorder (defectiveness) in the carbon within the composite.

Unlike the Raman spectrum of N, P-C, the spectrum of the V$_5$NP$_3$/N, P-C composite shows the appearance of peaks in the mid-frequency region (at 762, 927, and 1003 cm^{-1}) (Fig. 1b). The position and intensity of these peaks suggest they are due to the vibrations of V=O, V–O, and/or P–O bonds.[25–28] This, in turn, may indicate a partially oxidized state of the V$_5$NP$_3$ particles in the surface layer of the composite. However, according to X-ray diffraction data (Fig. 1a), this oxidation appears to occur only (or predominantly) on the surface of V$_5$NP$_3$/N, P-C and does not extend into the bulk of the composite.

As seen from the presented SEM images (Fig. 2), the obtained V$_5$NP$_3$/N, P-C composite consists of a carbon substrate with a sufficiently developed surface and submicron vanadium-containing particles of irregular shape dispersed on it. These particles primarily form agglomerates approximately 0.5–1.5 μm in size. From the TEM images of V$_5$NP$_3$/N, P-C (Fig. S1, SI) it is seen that the carbon component of the composite is inherently layered, and the majority of the V$_5$NP$_3$ particles (dark contrast) constituting the agglomerates are characterized by sizes of ∼50–100 nm. According to EDX data, the elemental composition (atomic %) of the obtained composite is: V – 1.33; N – 0.90; P – 0.98; C – 86.60; O – 10.19. The atomic ratios of N/V and P/V are greater than what is required to match the established phase composition of the composite, which is consistent with the assumption of N, P-doping of the carbon matrix.
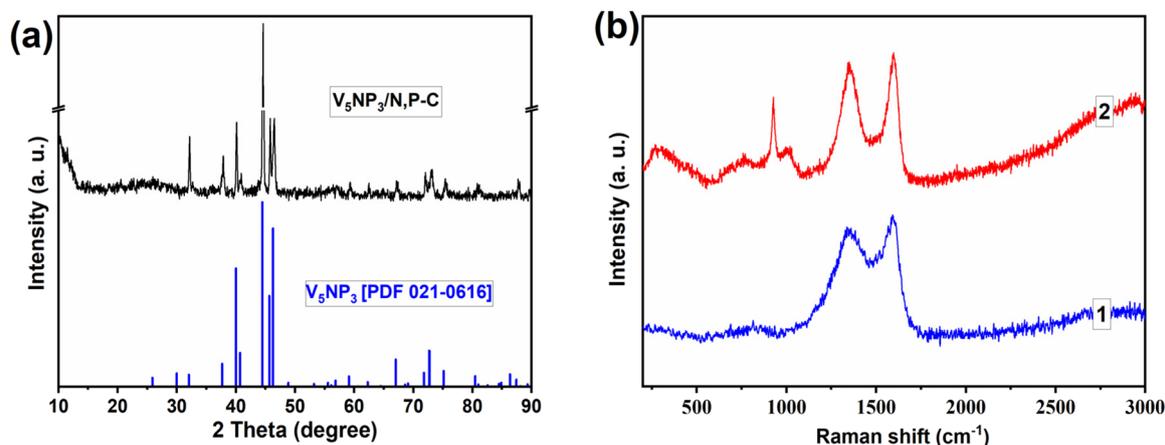

Fig. 1 (a) XRD-patterns of V$_5$NP$_3$/N, P-C and V$_5$NP$_3$ [PDF 021-0616], (b) Raman spectra of N, P-C (1) and V$_5$NP$_3$/N, P-C (2).

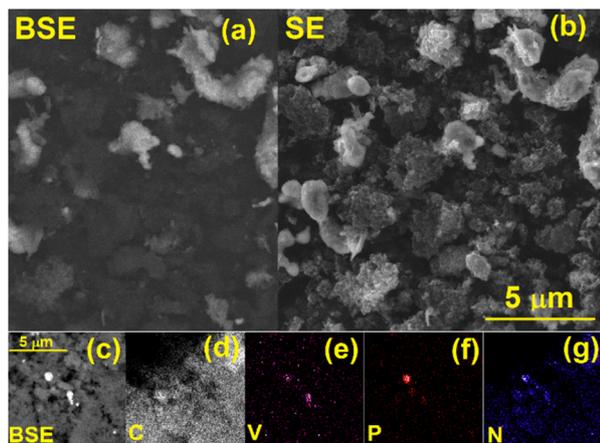© 2026 The Author(s). Published by the Royal Society of Chemistry

Fig. 2 SEM images of the V_5NP_3/N, P-C composite using back-scattered (BSE) (a) and secondary (SE) (b) electrons. Selected area (c) and corresponding elemental mappings for carbon (d), vanadium (e), phosphorus (f) and nitrogen (g).

The SEM selected area and the corresponding EDX elemental mapping images are shown in Fig. 2c–g. The images indicate that the V, P, and N elements are concentrated in regions corresponding to submicron particles distributed on the carbon substrate. This observation is consistent with the XRD data (Fig. 1a) which confirm the presence of vanadium

nitridophosphide as a component of the obtained V_5NP_3/N, P–C composite. Furthermore, the N and P elements are homogeneously distributed over the entire composite surface, suggesting successful doping of the carbon layer with nitrogen and phosphorus.

The presence of oxygen in the elemental composition of V_5NP_3/N, P-C, consistent with the results of Raman spectroscopy (Fig. 1b), could be a consequence of the composite's surface oxidation due to air exposure.[29,30] However, we cannot rule out the presence of a small amount of X-ray amorphous vanadium oxide phases within V_5NP_3/N, P-C, resulting from the incomplete reduction of oxygen-containing intermediates during the formation of V_5NP_3 particles *via* pyrolysis. The possible contribution of oxide impurities to the electrocatalytic properties of V_5NP_3/N, P-C, when considering the composite as a catalyst for HER, OER, and ORR, was not accounted for by us due to the difficulty of separating the contributions of individual components to the overall catalyst activity.

The surface chemical state of the elements present in the V_5NP_3/N, P-C was characterized by XPS. The high-resolution spectrum in the O 1s–V 2p region is shown in Fig. 3d. The presence of O 1s core level signal in the V 2p spectra is due to the oxidation of the composite surface, which usually occurs when the sample is in contact with air, including during the XPS test. The peak occurring at binding energy (BE) $\sim$529.2 eV can be attributed
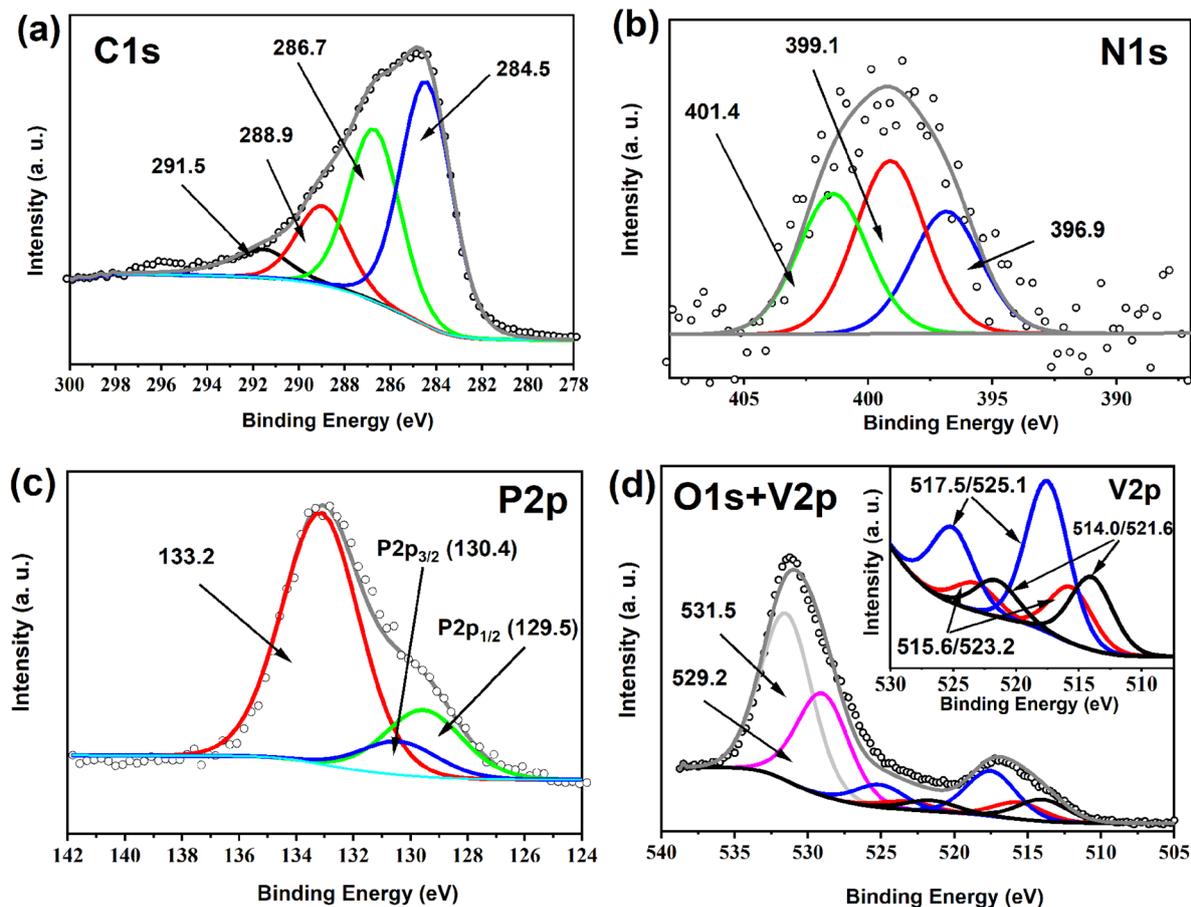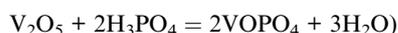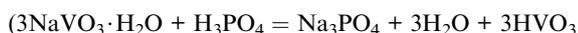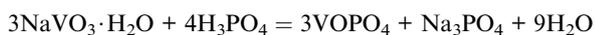

Fig. 3 XPS spectra of C 1s (a), N 1s (b), P 2p (c), O 1s and V 2p (inset – the result of the V2p spectrum deconvolution) (d) for V_5NP_3/N, P-C.

to the O–V bond, and at ∼531.4 eV to the hydroxyl group bonded to VN (O–V/O–H) or to the C=O fragments of the oxidized carbon component of the composite.[31–33] The V 2p spectrum after deconvolution shows three pairs of peaks (V $2p_{3/2}$/V $2p_{1/2}$) located at BEs of 514.0/521.6 (V–N/V–P bonding in V_5NP_3), 515.6/523.2 and 517.5/525.1 eV (Fig. 3b, inset), which are related to V^{3+} or V^{4+} (V–N–O/V–P–O), and V^{5+} (V–O), respectively, and are due to the partial oxidation of the surface of vanadium-containing particles of the composite.[31–34] Deconvolution of the N 1s spectrum of the composite (Fig. 3b) results in 3 peaks with maxima at 396.9 (N–V), 399.1 (pyridinic nitrogen) and 401.4 (graphitic nitrogen) eV,[34,35] which indicates the participation of nitrogen atoms in the formation of V-containing active sites of the catalyst and doping of the carbon substrate. It should be noted that the peak located in the BE region of ∼399 eV is also often attributed to oxidized nitrogen in the V–N–O fragment.[36,37] The P 2p spectrum (Fig. 3c) could be fitted into a doublet at 129.5 and 130.4 eV (corresponding to the binding energy of P $2p_{1/2}$ and P $2p_{3/2}$, respectively) as well as a peak at 133.2 eV. This doublet can be assigned to P–V bonding, while the high BE peak is attributed to P–O bond in O-containing groups (in particular, PO_4^{3-}) on the V_5NP_3 surface.[38–40] The high-resolution C 1s XPS spectrum of the catalyst (Fig. 3a) was decomposed into four components that can be attributed to sp^2 carbon (∼284.5 eV), structural fragments C–N/C–O/C–P (∼286.7 eV), C=O/C=N (∼288.9 eV), and also to $\pi \rightarrow \pi^*$ satellites of sp^2 graphitized carbon (∼291.5 eV).[35,41] This state of carbon is explained by the carbonization of the polymer during the formation of the catalyst, doping of the carbon matrix with nitrogen and, possibly, phosphorus atoms, as well as its partial oxidation.

Thus, considering the composition of the precursor and its heat treatment conditions, as well as the phase and elemental composition of the obtained composite, we can propose the following probable formation pathway for V_5NP_3/N, P-C, which is similar to that previously suggested for composites based on Ni, Co, Fe, and Mo phosphides obtained by an analogous approach.[18,19] During the formation of the precursor based on sodium metavanadate and PAni·H_3PO_4, $VOPO_4$ phosphate is formed, as established by X-ray diffraction method (Fig. S2, SI), due to the interaction between $NaVO_3 \cdot H_2O$ and H_3PO_4:

$$3NaVO_3 \cdot H_2O + 4H_3PO_4 = 3VOPO_4 + Na_3PO_4 + 9H_2O$$

$$(3NaVO_3 \cdot H_2O + H_3PO_4 = Na_3PO_4 + 3H_2O + 3HVO_3$$

$$2HVO_3 \rightarrow V_2O_5 + H_2O$$

$$V_2O_5 + 2H_3PO_4 = 2VOPO_4 + 3H_2O)$$

This is apparently due to the high phosphoric acid content in polyaniline, where it is present not only as a dopant but can also be additionally immobilized within the polymer matrix through specific adsorption.[20] With a further increase in pyrolysis temperature above 500 °C, PAni undergoes thermal degradation, leading to the carbonization of the polymer and the release of gaseous products (molecular hydrogen, ammonia).[42] Subsequently, via a carbothermal pathway,[43,44] the reduction of $VOPO_4$

occurs, resulting in the formation of the "phosphide" component in V_5NP_3. The product of the reduction of oxygen-containing phosphorus compounds – elemental phosphorus[45] – ensures the P-doping of the carbon matrix. Simultaneously, gaseous ammonia, a product of the polymer's thermal degradation, is responsible not only for the N-doping of carbon but also for the formation of the "nitride" component of V_5NP_3 through ammonification. This latter assumption is supported, in particular, by the known use of other nitrogen-containing polymers – poly-p-phenylenediamine[46] and poly-5-aminoindole[47] – as the sole nitrogen source in precursors for the formation of the Mo_2N phase within N-doped carbon composites under similar heat treatment conditions during their synthesis.

As mentioned above, the electrocatalytic properties of vanadium nitridophosphide or its composites in HER, OER, or ORR had not been previously investigated. Therefore, it was of interest to determine the activity of the obtained V_5NP_3/N, P-C composite in these processes and compare it with the electrocatalytic characteristics attributed to literature-described catalysts based on phosphides and vanadium nitride (in the absence of additional late d-metals in their composition), as well as N, P-C and Pt/C catalysts.

As a result of studies conducted using linear sweep voltammetry, the ability of V_5NP_3/N, P-C to exhibit electrocatalytic activity in HER was established in both acidic (Fig. 4a) and alkaline (Fig. 4b) electrolytes. Hydrogen evolution on the V_5NP_3/N, P-C catalyst occurs at significantly lower potentials than on N, P-C, indicating that the V_5NP_3 particles are the primary active sites of the obtained composite electrocatalyst in HER.

The onset potential (E_{onset}) is an important indicator for comparing the efficiency of catalysts in HER. A more effective catalyst for this electrochemical process exhibits a lower (i.e., more positive) E_{onset}, since less voltage is required for HER initiation. As can be seen from the data presented in Table 1, V_5NP_3/N, P-C demonstrated a more positive E_{onset} (was defined as the potential at which the cathodic current density reaches 1 mA cm^{-2}) compared to N, P-C (by 165 mV in 1.0 M NaOH and by 235 mV in 0.5 M H_2SO_4), indicating its significantly higher activity in HER. For both catalysts, E_{onset} undergoes a cathodic shift when switching from an acidic to an alkaline electrolyte (Table 1). However, for V_5NP_3/N, P-C, this shift is much considerably smaller (31 mV) compared to N, P-C (165 mV).

If we consider the hydrogen evolution overpotential at a current density of 10 mA cm^{-2} (η_{10}) and the Tafel slope (b) as criteria for catalyst activity, then the efficiency of V_5NP_3/N, P-C in both aqueous 0.5 M H_2SO_4 and 1.0 M NaOH is comparable (Fig. 4 and Table 1). In these electrolytes, the catalyst exhibits identical b values and only a minor difference in η_{10} values (approximately 21 mV). Based on the calculated b value (∼91 mV dec^{-1}), it can be assumed that hydrogen evolution on the V_5NP_3/N, P-C catalyst proceeds via the Volmer–Heyrovsky mechanism,[48] with the Volmer step being the rate-limiting step.

It is worth noting that the difference in η_{10} and b values between V_5NP_3/N, P-C and N, P-C is significantly larger in acidic electrolyte (315 mV and 85 mV dec^{-1}) than in alkaline electrolyte (218 mV and 69 mV dec^{-1}) (Table 1). This could be attributed to the higher activity of N, P-C in HER specifically at high
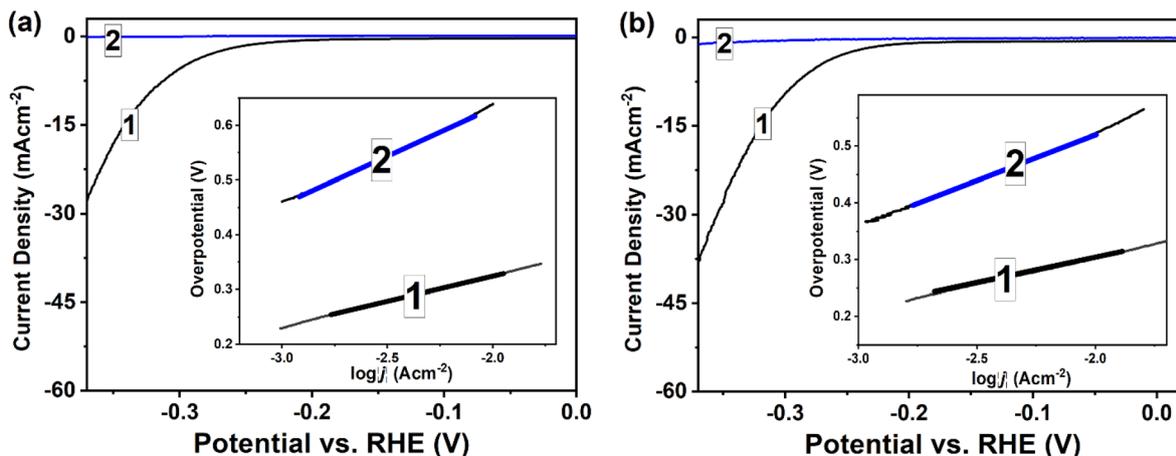
Fig. 4 HER polarization curves and Tafel plots (insets) obtained in 0.5 M H_2SO_4 (a) and 1.0 M NaOH (b) for GC electrodes modified with V_5NP_3/N, P-C (1) and N, P-C (2). Potential scan rate: 5 mV s^{-1}.

Table 1 Main HER parameters for V_5NP_3/N, P-C, N, P-C, and Pt/C in electrolytes with different pH

	b, mV dec^{-1}	η_{10}, mV	E_{onset}, mV	j_0, mA cm^{-2}
0.5 M H_2SO_4				
V_5NP_3/N, P-C	91	325	−228	2.9×10^{-3}
N, P-C	176	640	−463	2.7×10^{-3}
Pt/C	21	43	0	1.2×10^{-1}
1.0 M NaOH				
V_5NP_3/N, P-C	91	304	−197	5.9×10^{-3}
N, P-C	160	522	−358	5.4×10^{-3}
Pt/C	38	21	0	2.3

pH, primarily due to the presence of CN_x-centers in such catalysts.[49]

Regardless of the electrolyte type, V_5NP_3/N, P-C is considerably inferior to Pt/C catalyst in terms of both η_{10} overpotential and Tafel slope. This is not unexpected and is characteristic of catalysts based on vanadium nitride or phosphides when late d-metals are absent from their composition (Table S1, SI). Specifically, the limited productivity of VN in HER is linked to the exceptionally strong Gibbs free energy of hydrogen adsorption (ΔG_{H*}) inherent to this nitride.[50,51] It is possible that the same effect occurs for V_5NP_3/N, P-C. However, the electrocatalytic activity in HER of our obtained composite (considering the calculated η_{10} and b values) surpasses that of most known analogs based on VN and VP (Table S1, SI). This might be a result of the combination of "nitride" and "phosphide" components within V_5NP_3/N, P-C, which possibly contributes to optimal hydrogen adsorption on this catalyst, thereby improving its efficiency in HER.

Along with the η_{10} overpotential and Tafel slope, the exchange current density (j_0) is also used to compare the performance of catalysts in HER. As a kinetic parameter, j_0 reflects the intrinsic activity of a catalyst under equilibrium conditions. The j_0 values for V_5NP_3/N, P-C and N, P-C catalysts presented in Table 1 were calculated by extrapolating the corresponding Tafel plots to zero

overpotential. Since V_5NP_3/N, P-C exhibits higher j_0 values than N, P-C in both electrolytes used, this indicates its higher electrocatalytic activity in HER due to more efficient electron transfer at the electrode/electrolyte interface.

The electrochemically active surface area (ECSA) of V_5NP_3/N, P-C and N, P-C was estimated based on the double-layer capacitance values of the electrodes modified with the corresponding catalysts calculated from cyclic voltammograms (CVs) recorded at different scan rates (5, 10, 20, 40, 60, 80, and 100 mV s^{-1}) between 0.05 and 0.15 V in 0.5 M H_2SO_4 and 1.0 M NaOH (Fig. S3a, b, d and e, SI). The potential regions were chosen to avoid interference of pseudocapacitances caused by surface redox reactions. As shown in the Fig. S3c and f a linear correlation is observed when the current density at 0.1 V is plotted against the scan rate. Based on the linear fittings (Fig. S3c, SI) the mass specific capacitance of the catalysts (C) (eqn (1)) was determined, as follows:[52]

$$C = k/2m \qquad (1)$$

where C is the mass specific capacitance of catalyst, k is the fitting slope (136.8 and 24.3 mF cm^{-2} in 0.5 M H_2SO_4, 156.0 and 46.0 mF cm^{-2} in 1.0 M NaOH for V_5NP_3/N, P-C and N, P-C, respectively), m is the catalyst areal loading (1.15 mg cm^{-2}).

The C values obtained from eqn (1) are 59.5 (0.5 M H_2SO_4) and 67.8 (1.0 M NaOH) F g^{-1} for V_5NP_3/N, P-C, as well as 10.6 (0.5 M H_2SO_4) and 20.0 (1.0 M NaOH) F g^{-1} for N, P-C. Based on these, the ECSA of V_5NP_3/N, P-C and N, P-C was calculated (eqn (2)).[52] The specific capacitance (C_s) (eqn (2)) was chosen as 0.035 (0.5 M H_2SO_4) and 0.030 (1.0 M NaOH) mF cm^{-2} based on typical values reported for the indicated electrolytes.[53]

$$\text{ECSA} = C/C_s \qquad (2)$$

Estimated values of ECSA are 170.0 (0.5 M H_2SO_4) and 226.0 (1.0 M NaOH) m^2 g^{-1} for V_5NP_3/N, P-C as well as 30.3 (0.5 M H_2SO_4) and 66.6 (1.0 M NaOH) m^2 g^{-1} for N, P-C. The results show that the ECSA of composite electrocatalyst was much

higher than that of N, P-C, indicating that V_5NP_3/N, P-C had more active sites toward HER, in particular.

In addition, the electrochemical impedance spectroscopy (EIS) measurements were carried out to estimate the charge transfer ability of the obtained catalysts. As shown in Fig. S4a and b (SI) Nyquist plots, the V_5NP_3/N, P-C possess much lower charge transfer resistance compared to the N, P-C, indicating higher conductivity and faster electron transfer between composite electrode and electrolyte (0.5 M H_2SO_4 or 1.0 M NaOH). This suggests that the presence of V_5NP_3 in the composite is beneficial to charge-carrier transportation, thus improving the catalytic performance. The smaller ratio between the sizes of the semicircles for V_5NP_3/N, P-C and N, P-C in the Nyquist plots recorded in 1.0 M NaOH, compared with those in 0.5 M H_2SO_4 (Fig. S4a and b, SI), is consistent with the difference in the activity of the obtained catalysts in alkaline and acidic electrolytes (Table 1).

Electrochemical stability is an important criterion for evaluating the performance of electrocatalysts. The long-term durability of V_5NP_3/N, P-C in HER was estimated by chronopotentiometry test at the constant current density of 10 mA cm^{-2} in 0.5 M H_2SO_4 and 1.0 M NaOH. As can be seen from the chronopotentiometry plots (Fig. S5a, SI), overpotential value (η_{10}) for obtained catalyst increases by ∼9% and ∼18% of its initial ones after 8 h of continuous operation in alkaline and acid electrolyte, respectively. On repeated recording of the HER polarization curves after electrolysis for 8 h, a slight cathodic shift is observed for them ($\Delta\eta_{10} \sim$ 25 and 51 mV in 1.0 M NaOH and 0.5 M H_2SO_4, respectively) (Fig. S5b and c, SI), indicating minor catalyst degradation.

Alongside HER, the obtained hybrid catalyst V_5NP_3/N, P-C also exhibits activity in the oxygen evolution reaction (OER) in 1.0 M NaOH (Fig. 5). In this process, it is characterized by E_{onset} 1.233 V (was defined as the potential at which the anodic current density reaches 1 mA cm^{-2}), η_{10} value of approximately 290 mV and a Tafel slope (b) of approximately 241 mV dec^{-1}. It's important to note that, according to current understanding, vanadium compounds other than oxides/hydroxides do not directly act as active sites in OER; instead, they serve as pre-catalysts.[17] Under anodic conditions, a shell of amorphous mixed vanadium hydroxides and oxides forms on the V-containing particles (the core),[54] and the presence of this shell is what drives the electrocatalytic effect in OER. Considering that the obtained V_5NP_3/N, P-C provides a significantly lower oxygen evolution overpotential in OER compared to known systems based on VN or VP (Table S2, SI), we can hypothesize several possibilities: a higher efficiency in the formation of the hydroxide/oxide surface layer specifically on the vanadium nitridophosphide particles, or higher electrical conductivity of V_5NP_3, which accelerates electron transfer between the core and the shell, or a synergistic catalytic effect between the core (V_5NP_3) and the shell.[55] To assess the efficiency of V_5NP_3/N, P-C and N, P-C in OER, EIS measurements were also performed at a potential of 1.6 V. The resulting Nyquist plots are shown in Fig. S4c (SI). At the measured potential and frequency range N, P-C demonstrates only capacitive behavior, which causes its inefficiency as an OER catalyst. At the same time, a typical semicircle in Nyquist plot due to the charge transfer processes, in particular, occurs for V_5NP_3/N, P-C. This difference in the shape of the Nyquist plots is consistent with the dramatic differences in the manifestation of activity in OER between V_5NP_3/N, P-C and N, P-C (Fig. 5a).

To evaluate the electrocatalytic activity of the obtained hybrid material in ORR, electrochemical studies were conducted using the rotating ring-disk electrode (RRDE) method on GC electrodes modified with V_5NP_3/N, P-C, as well as, for comparison, N, P-C and Pt/C. The polarization curves for oxygen reduction on these catalysts, obtained in an alkaline electrolyte, are shown in Fig. 6. As the figure illustrates, V_5NP_3/N, P-C is significantly more effective in ORR compared to N, P-C, indicating the key role of V_5NP_3 particles in the composite as catalytically active centers. However, as expected, its activity is inferior to that of the Pt-based catalyst.

Table 2 presents the main ORR parameters for V_5NP_3/N, P-C, N, P-C, and Pt/C catalysts, calculated from RRDE data. Notably, V_5NP_3/N, P-C as an ORR catalyst exhibits a relatively
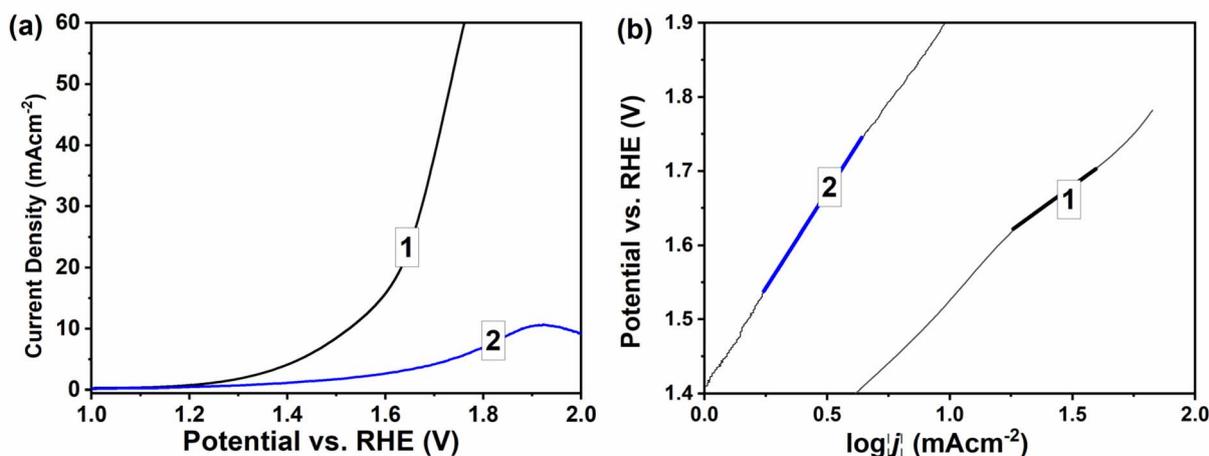

Fig. 5 (a) OER polarization curves and (b) Tafel plots obtained for GC electrodes modified with V_5NP_3/N, P-C (1) and N, P-C (2). Electrolyte: 1.0 M NaOH; potential scan rate: 5 mV s^{-1}.
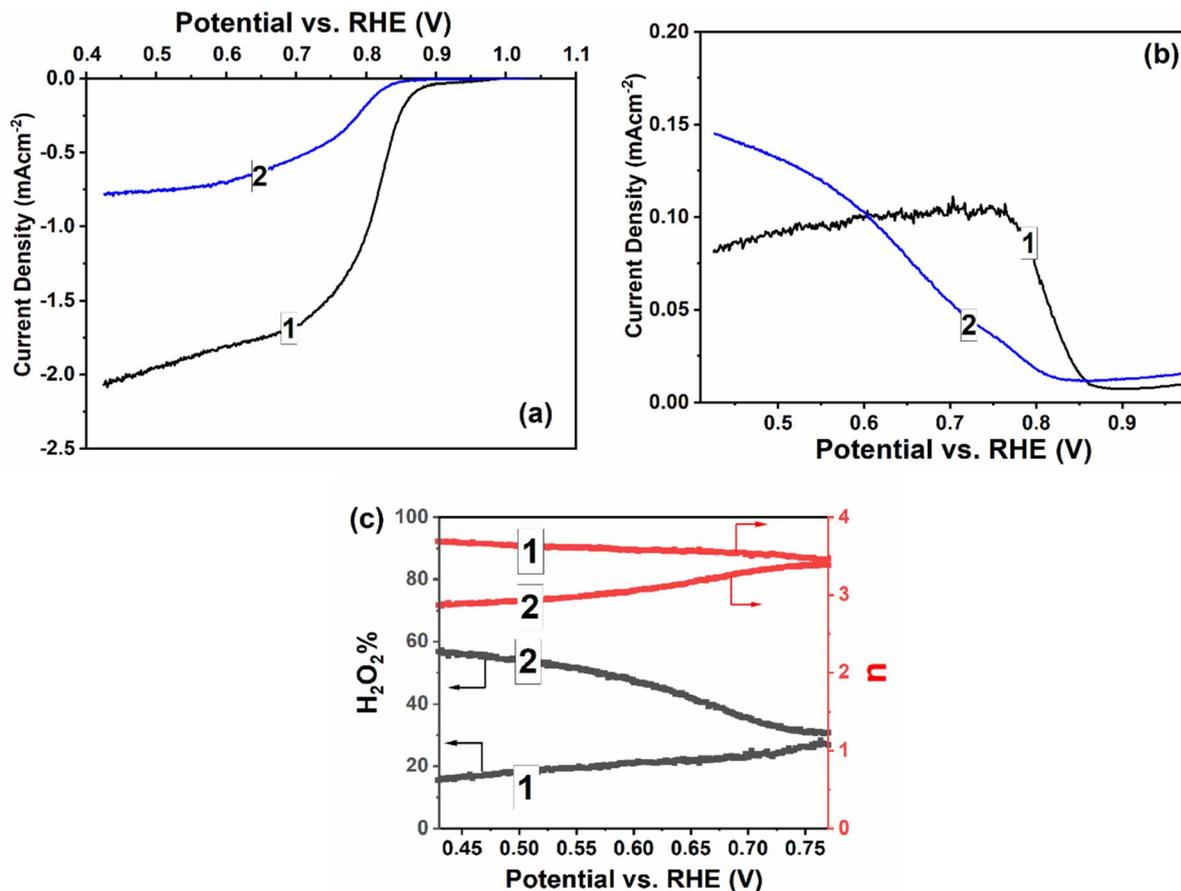
Fig. 6 (a) ORR polarization curves for a GC electrode modified with V_5NP_3/N, P-C (1) and N, P-C (2) in oxygen-saturated 1.0 M NaOH at a rotation speed of 1200 rpm. (b) Corresponding J_r–E_d dependencies obtained at a Pt-ring polarization potential of 1000 mV; the potential scan rate 5 mV s^{-1} (c) The H_2O_2%-E_d and n–E_d dependences for the V_5NP_3/N, P-C (1) and N, P-C (2) catalysts.

high E_{onset} of 0.89 V (was defined as the potential at which the cathodic current density reaches 0.05 mA cm^{-2}) and a half-wave potential ($E_{1/2}$) of 0.82 V, which are about 50 mV higher than those for N, P-C (Table 2). Another advantage of V_5NP_3/N, P-C over N, P-C in ORR is a more than twofold lower average hydrogen peroxide yield (H_2O_2%), which is an undesirable product of this process. Given the established average number of electrons (n) participating in oxygen molecule reduction for the studied catalysts (Table 2), ORR on V_5NP_3/N, P-C primarily proceeds *via* a 4-electron mechanism, with a minor contribution from a 2-electron pathway, whereas the contribution of 2- and 4-electron mechanisms to oxygen reduction on N, P-C is comparable.

It is important to note that the hydrogen peroxide yield and, accordingly, n depend significantly on the value of the potential applied to the working electrode (E_d). Moreover, the H_2O_2%-E_d and n–E_d dependences for the V_5NP_3/N, P-C and N, P-C catalysts are fundamentally different (Fig. 6c). At high potentials (~0.74–0.76 V), the H_2O_2% and n values are close for both catalysts. However, with an increase in overpotential, there is a sharp increase in the yield of H_2O_2 in ORR for N, P-C (from ~32% at E = 0.74 V to ~57% at E = 0.43 V), while for V_5NP_3/N, P-C, on the contrary, there is a slight monotonic decrease in H_2O_2% (from ~25% at E = 0.74 V to ~16% at E = 0.43 V). This is

Table 2 Main ORR parameters for V_5NP_3/N, P-C, N, P-C, and Pt/C catalysts, calculated from RRDE measurements in oxygen-saturated 1.0 M NaOH at an electrode rotation speed of 1200 rpm

	E_{onset}, V	$E_{1/2}$, V	n	H_2O_2%	b, mV dec^{-1}
V_5NP_3/N, P-C	0.89	0.82	3.58	21.0	61
N, P-C	0.84	0.77	3.09	45.0	38
Pt/C	0.97	0.91	3.96	1.9	51

in complete agreement with the corresponding n–E_d dependences (Fig. 6c).

In terms of E_{onset} and $E_{1/2}$ values, V_5NP_3/N, P-C surpasses known ORR catalysts based on VN (Table S3, SI), provided that the latter do not contain additional late d-metals. Compared to VN-containing catalysts, V_5NP_3/N, P-C also features a lower Tafel slope (b) in ORR (Table S3, SI), which may indicate more favorable kinetics for oxygen reduction, leading to higher productivity in this process. Unfortunately, we haven't found information on the ORR characteristics of systems based on vanadium phosphides, which prevents their comparison with V_5NP_3/N, P-C as oxygen reduction electrocatalysts.

To characterize the durability of V_5NP_3/N, P-C in ORR, it was further estimated by chronoamperometry test with the potential

holding at 0.6 V in O_2-saturated 1.0 M NaOH. As can be seen from the chronoamperometric response (Fig. S6, SI), the V_5NP_3/N, P-C catalyst retained ~90% of the initial current after 8 h, thereby showing sufficiently high stability to ORR.

The catalytically active sites involved in the studied processes are fundamentally different in the case of V_5NP_3/N, P-C and N, P-C. The established significant improvement in the electrocatalytic performance of V_5NP_3/N, P-C compared to N, P-C may, first of all, be a consequence of the intrinsic activity of vanadium-containing particles that are present in the composite and absent in N, P-C. Also, in the case of OER, the presence of metal-containing particles in the composite determines the possibility of the formation of the hydroxide/oxide layer on their surface, which provides much higher catalytic characteristics in the specified process compared to N, P-C, where this possibility is absent. Although the activity of N, P-C itself in the processes under consideration is low, it is impossible to exclude the positive contribution of the carbon component to the overall activity of the composite, in particular, due to the manifestation of a synergistic effect. The improvement of the electrocatalytic performance of V_5NP_3/N, P-C compared to N, P-C is also consistent with the established better charge transfer ability and higher ECSA specifically for the composite.

It should be noted that while the electrocatalytic activity of V_5NP_3/N, P-C in HER, OER, and ORR is moderate, the observed functional advantages of the obtained hybrid material over systems based on vanadium nitride and phosphides as catalysts for these processes (Tables S1–3, SI) suggest that further strategies could significantly enhance its performance. Specifically, incorporating late d-metal doping into V_5NP_3 within our proposed approach, combining V_5NP_3 with phosphides (nitrides) of Co, Ni, Fe, and implementing other known modification strategies, could lead to competitive electrocatalytic characteristics for V_5NP_3-based materials in the discussed reactions.

Conclusions

Thus, we have for the first time synthesized a hybrid composite based on vanadium nitridophosphide and N, P-doped carbon (V_5NP_3/N, P-C) through the pyrolysis of a precursor made from H_3PO_4-doped polyaniline and $NaVO_3$. This proposed carbothermal approach is straightforward to implement and avoids the need for toxic phosphorus compounds.

We've established that V_5NP_3/N, P-C exhibits electrocatalytic properties in HER: ($\eta_{10} \sim 304$ mV, $b \sim 91$ mV dec^{-1} in 1.0 M NaOH; and $\eta_{10} \sim 325$ mV, $b \sim 91$ mV dec^{-1} in 0.5 M H_2SO_4), OER ($\eta_{10} \sim 290$ mV and $b \sim 241$ mV dec^{-1}) and ORR ($E_{onset} \sim 890$ mV, $E_{1/2} \sim 820$ mV, and $b \sim 61$ mV dec^{-1}). Furthermore, in the most cases, V_5NP_3/N, P-C surpasses the activity of known catalysts based on vanadium nitride or phosphides (that lack additional late d-metals) in these processes. This high performance may stem from the combination of "nitride" and "phosphide" components within the obtained composite. It's also been shown that V_5NP_3 particles play a crucial role as the catalytically active centers in the composite, providing significantly higher efficiency

for V_5NP_3/N, P-C in the discussed reactions compared to N, P-C, which lacks vanadium-containing particles.

Author contributions

D. O. M.: methodology, experimental data production, analysis of the obtained results, and preparation of manuscript materials. O. O. P.: experimental data production and analysis of the obtained results. Y. I. K.: conceptualization, methodology, analysis, and generalization of the obtained results, writing of the original manuscript. V. G. K.: conceptualization, discussion of results, manuscript editing, and guidance.

Conflicts of interest

There are no conflicts of interest to declare.

Data availability

The data supporting this study's findings are available in the main text and supplementary information (SI). Supplementary information is available. See DOI: https://doi.org/10.1039/d5ra05349h.

Acknowledgements

Notes and references

1 W. Li, H. Tian, L. Ma, Y. Wang, X. Liu and X. Gao, *Mater. Adv.*, 2022, **3**, 5598–5644.

2 V. Vij, S. Sultan, A. M. Harzandi, A. Meena, J. N. Tiwari, W.-G. Lee, T. Yoon and K. S. Kim, *ACS Catal.*, 2017, **7**, 7196–7225.

3 T. Ingsel, F. M. de Souza and R. K. Gupta, in *Noble Metal-free Electrocatalysts: Fundamentals and Recent Advances in Electrocatalysts for Energy Applications. Volume 1*, American Chemical Society, 2022, vol. 1431, pp. 1–29.

4 W. Sheng, H. A. Gasteiger and Y. Shao-Horn, *J. Electrochem. Soc.*, 2010, **157**, B1529.

5 R. Kuriki, O. Ishitani and K. Maeda, *ACS Appl. Mater. Interfaces*, 2016, **8**, 6011–6018.

6 V. Pfeifer, T. E. Jones, J. J. V. Vélez, R. Arrigo, S. Piccinin, M. Hävecker, A. Knop-Gericke and R. Schlögl, *Chem. Sci.*, 2017, **8**, 2143–2149.

7 M. Carmo, D. L. Fritz, J. Mergel and D. Stolten, *Int. J. Hydrogen Energy*, 2013, **38**, 4901–4934.

8 X. Zou and Y. Zhang, *Chem. Soc. Rev.*, 2015, **44**, 5148–5180.

9 M. A. Khan, H. Zhao, W. Zou, Z. Chen, W. Cao, J. Fang, J. Xu, L. Zhang and J. Zhang, *Electrochem. Energy Rev.*, 2018, **1**, 483–530.

10 C. Hu and L. Dai, *Angew. Chem., Int. Ed.*, 2016, **55**, 11736–11758.

11 J. Li, Z. Zhao, Y. Ma and Y. Qu, *ChemCatChem*, 2017, **9**, 1554–1568.

12 J. Wang, F. Xu, H. Jin, Y. Chen and Y. Wang, *Adv. Mater.*, 2017, **29**, 1605838.

13 C. Huang, P. Qin, Y. Luo, Q. Ruan, L. Liu, Y. Wu, Q. Li, Y. Xu, R. Liu and P. K. Chu, *Mater. Today Energy*, 2022, **23**, 100911.

14 L. Huo, C. Jin, K. Jiang, Q. Bao, Z. Hu and J. Chu, *Adv. Energ. Sust. Res.*, 2022, **3**, 2100189.

15 N. Mahmood, Y. Yao, J.-W. Zhang, L. Pan, X. Zhang and J.-J. Zou, *Adv. Sci.*, 2018, **5**, 1700464.

16 W.-F. Chen, J. T. Muckerman and E. Fujita, *Chem. Commun.*, 2013, **49**, 8896–8909.

17 H. Li, J. Wu, M. Li and Y. Wang, *Catalysts*, 2024, **14**, 368.

18 D. O. Mazur, O. O. Pariiska, Y. I. Kurys, V. G. Koshechko and V. D. Pokhodenko, *J. Electrochem. Soc.*, 2024, **171**, 076506.

19 D. O. Mazur, O. O. Pariiska, Ya. I. Kurys, V. G. Koshechko and V. D. Pokhodenko, *Theor. Exp. Chem.*, 2024, **60**, 177–184.

20 N. V. Blinova, J. Stejskal, M. Trchová and J. Prokeš, *Polymer*, 2006, **47**, 42–48.

21 H. Boller and H. Nowotny, *Monatsh. Chem.*, 1968, **99**, 672–675.

22 Q. Shi, Q. Liu, Y. Zheng, Y. Dong, L. Wang, H. Liu and W. Yang, *Energy Environ. Mater.*, 2022, **5**, 515–523.

23 Y. Liu, X. Guan, B. Huang, Q. Wei and Z. Xie, *Front. Chem.*, 2020, **7**, 805.

24 M. Zhuang, X. Ou, Y. Dou, L. Zhang, Q. Zhang, R. Wu, Y. Ding, M. Shao and Z. Luo, *Nano Lett.*, 2016, **16**, 4691–4698.

25 P. Shvets, K. Maksimova and A. Goikhman, *Phys. B*, 2021, **613**, 412995.

26 T. P. Moser and G. L. Schrader, *J. Catal.*, 1985, **92**, 216–231.

27 R. L. Frost, K. L. Erickson, M. L. Weier and O. Carmody, *Spectrochim. Acta, Part A*, 2005, **61**, 829–834.

28 F. Ben Abdelouahab, R. Olier, N. Guilhaume, F. Lefebvre and J. C. Volta, *J. Catal.*, 1992, **134**, 151–167.

29 G.-H. An, D.-Y. Lee and H.-J. Ahn, *J. Mater. Chem. A*, 2017, **5**, 19714–19720.

30 P. Zhou, D. Xing, Y. Liu, Z. Wang, P. Wang, Z. Zheng, X. Qin, X. Zhang, Y. Dai and B. Huang, *J. Mater. Chem. A*, 2019, **7**, 5513–5521.

31 C. M. Ghimbeu, E. Raymundo-Piñero, P. Fioux, F. Béguin and C. Vix-Guterl, *J. Mater. Chem.*, 2011, **21**, 13268–13275.

32 b Q. Yang, Z. Wang, F. Shi, D. Li, Y. Peng and J. Liu, *RSC Adv.*, 2025, **15**, 23994–24001.

33 J. Kasten, C.-C. Hsiao, D. Johnson and A. Djire, *Nanoscale Adv.*, 2023, **5**, 3485–3493.

34 Y. Fu, L. Han, P. Zheng, X. Peng, X. Xian, J. Liu, X. Zeng, P. Dong, J. Xiao and Y. Zhang, *Catalysts*, 2022, **12**, 877.

35 N. Zhang, L. Cao, L. Feng, J. Huang, K. Kajiyoshi, C. Li, Q. Liu, D. Yang and J. He, *Nanoscale*, 2019, **11**, 11542–11549.

36 H. M. Morales, H. Vieyra, D. A. Sanchez, E. M. Fletes, M. Odlyzko, T. P. Lodge, V. Padilla-Gainza, M. Alcoutlabi and J. G. Parsons, *Int. J. Mater. Sci.*, 2024, **25**, 6952.

37 M. Chen, H. Fan, Y. Zhang, X. Liang, Q. Chen and X. Xia, *Small*, 2020, **16**, 2003434.

38 P. Wei, Q. Geng, A. I. Channa, X. Tong, Y. Luo, S. Lu, G. Chen, S. Gao, Z. Wang and X. Sun, *Nano Res.*, 2020, **13**, 2967–2972.

39 X. Xu, Y. Lu, J. Shi, X. Hao, Z. Ma, K. Yang, T. Zhang, C. Li, D. Zhang, X. Huang and Y. He, *Nat. Commun.*, 2023, **14**, 7708.

40 X. Zhang, T. Guo, X. Cao, C. Ma, J. Yan and R. Liu, *J. Alloys Compd.*, 2022, **920**, 165932.

41 O. Pariiska, D. Mazur, Y. Kurys, R. Socha, V. Koshechko and V. Pokhodenko, *J. Solid State Electrochem.*, 2021, **25**, 2309–2319.

42 M. K. Traore, W. T. K. Stevenson, B. J. McCormick, R. C. Dorey, S. Wen and D. Meyers, *Synth. Met.*, 1991, **40**, 137–153.

43 P. Liang, F. Liang, Z. Yao, H. Gao, Y. Sun, B. Jiang and J. Tong, *Phosphorus Sulfur Silicon Relat. Elem.*, 2017, **192**, 812–818.

44 Z. Yao, H. Hai, Z. Lai, X. Zhang, F. Peng and C. Yan, *Top. Catal.*, 2012, **55**, 1040–1045.

45 J. Sun, H.-W. Lee, M. Pasta, Y. Sun, W. Liu, Y. Li, H. R. Lee, N. Liu and Y. Cui, *Energy Storage Mater.*, 2016, **4**, 130–136.

46 Y.-J. Song and Z.-Y. Yuan, *Electrochim. Acta*, 2017, **246**, 536–543.

47 Y. I. Kurys, D. O. Mazur, V. G. Koshechko and V. D. Pokhodenko, *Electrocatalysis*, 2021, **12**, 469–477.

48 T. Shinagawa, A. T. Garcia-Esparza and K. Takanabe, *Sci. Rep.*, 2015, **5**, 13801.

49 G. Long, K. Wan, M. Liu, Z. Liang, J. Piao and P. Tsiakaras, *J. Catal.*, 2017, **348**, 151–159.

50 P. Zhou, D. Xing, Y. Liu, Z. Wang, P. Wang, Z. Zheng, X. Qin, X. Zhang, Y. Dai and B. Huang, *J. Mater. Chem. A*, 2019, **7**, 5513–5521.

51 X. Yu, F. Cheng and K. Xie, *New J. Chem.*, 2022, **46**, 1392–1398.

52 Y. Huang, Q. Gong, X. Song, K. Feng, K. Nie, F. Zhao, Y. Wang, M. Zeng, J. Zhong and Y. Li, *ACS Nano*, 2016, **10**, 11337–11343.

53 C. C. L. McCrory, S. Jung, J. C. Peters and T. F. Jaramillo, *J. Am. Chem. Soc.*, 2013, **135**, 16977–16987.

54 H. Yang, Y. Hu, D. Huang, T. Xiong, M. Li, M.-S. Balogun and Y. Tong, *Mater. Today Chem.*, 2019, **11**, 1–7.

55 L.-A. Stern, L. Feng, F. Song and X. Hu, *Energy Environ. Sci.*, 2015, **8**, 2347–2351.